Saudi Journal of Biological Sciences (2016) 23, S126–S136

King Saud University

Saudi Journal of Biological Sciences

www.ksu.edu.sa
www.sciencedirect.com

ORIGINAL ARTICLE

Mechanical characteristics of antibacterial epoxy resin adhesive wood biocomposites against skin disease

Zi-xiang Chen [a], Zhong-feng Zhang [a,*], Wan Syaidatul Aqma [b]

[a] Furniture and Art College, Central South University of Forestry and Technology, Changsha City 410004, China
[b] School of Biosciences and Biotechnology, Faculty of Science and Technology, Universiti Kebangsaan Malaysia, 43600 Bangi, Selangor, Malaysia

Received 8 July 2015; revised 10 September 2015; accepted 14 September 2015
Available online 9 October 2015

KEYWORDS

Antibacterial effect;
EP/wood biocomposites;
Skin disease;
Reinforced effect

Abstract Moldy wood can cause some skin disease. However epoxy resin adhesive (EP) can inhibit mold growth. Therefore, antibacterial EP/wood biocomposites were reinforced and analyzed by the nonlinear finite element. Results show that glass fiber cloth and aluminum foil have the obvious reinforced effect under flat pressure, but this was not the case under side pressure. And when the assemble pattern was presented in 5A way, the strengthening effect was better. The nonlinear finite element showed that the aluminum foil and glass fiber cloth have the obvious reinforced effect. The mutual influence and effect of span, thickness and length on the ultimate bearing capacity of specimen were studied. And the simulation results agreed with the test. It provided a theoretical basis on the preparation of antibacterial EP/wood biocomposites against skin disease.

1. Introduction

This painful viral infection is caused by herpes zoster, the virus that causes chickenpox. After infection with chickenpox, the virus "hides" in the nervous system in a latent or dormant state. Exposure to chickenpox or other stressors may cause a reactivation of the virus, resulting in a shingles outbreak. People over the age of 50 are most likely to suffer from shingles (Xiao et al., 2013).

Shingles causes uncomfortable and painful symptoms due to inflammation of the sensory nerves, the nerves responsible for the perception of pain, touch, and temperature. The characteristic shingles rash appears as a band-like strip of red, oozing blisters. The rash typically wraps in a strip around the body and usually occurs on one side of the body. Shingles is contagious if an infected person has close contact with others who have not yet had chickenpox. Nerve pain due to shingles can sometimes persist for weeks to years after the rash heals. This painful, post viral condition is known as post-herpetic neuralgia. Some researches showed the herpes zoster came from moldy wood (Mateen et al., 2015).

* Corresponding author.
E-mail address: csfuzzf@163.com (Z.-f. Zhang).
Peer review under responsibility of King Saud University.

Production and hosting by Elsevier

http://dx.doi.org/10.1016/j.sjbs.2015.09.026

Insects and mold can damage wood over time. To prevent that damage, wood is often treated with pesticides (Barreto et al., 2010). Treated wood is commonly used to build telephone poles, road signs and marine pilings as well as decks, play structures and raised garden beds (Hernandez et al., 1997). Several wood preservatives are registered with the EPA, each with different uses and potential risks (Yin et al., 2001).

Wood preservatives can extend the life of wood and reduce the need for forest resources, but proper use is important (Peng et al., 2011, 2012a,b; Peng and Le, 2012). Some preservatives can slowly leach into the surrounding soil or water. Sometimes, touching the wood can leave a residue on exposed skin. Use the resources below to learn about selecting and using treated wood properly. Wood extractives contain plenty of nutrients and hormones (Qureshi et al., 2015). What's more, resin can strengthen and inhibit the wood mildew (Rasheed et al., 2015). Therefore, the antibacterial EP/wood biocomposites were reinforced and analyzed by the nonlinear finite element.

2. Material and methods

2.1. Test materials

Eucalyptus plantation wood veneer, with the format of 1.27 m × 0.64 m × 1.3 mm, the density of about 0.61 g/cm^3 and the water content of 5–8% was used.

Epoxy resin adhesive double component epoxy adhesive, of which the component A is the milky white to pale yellow viscous liquid and the component B is the yellowish brown to reddish brown viscous liquid. The working life is 1 h (25 °C), curing speed is 2.5–3.5 h (25 °C), tensile shear strength ⩾8 MPa (25 °C × 48 h) (Youngquist et al., 1979).

Glass fiber cloth, plain weave, with the warp and weft density of 128 × 68 was used.

2.2. Specimen design scheme

The design of the experiment is shown in Table 1. There are 5 groups of solutions in all, and each group has 3 parallel specimens. By comparing the schemes of 1A, 2A, 3A, and 5A, the enhancement effect of glass fiber cloth can be revealed; by comparing the schemes of 1A, 2A, 4A, and 5A, the enhancement effect of aluminum foil can be revealed.

2.3. Test methods

Assembling was done in accordance with the assemble patterns shown in Table 1 , with the double-sided glue consumption of 350 g/cm^2.After assembling, it was put into the compressor under the temperature of about 20 °C, and then pressure was raised to 4 MPa. After applying the pressure for 1 h, the power was turned off and the pressure was applied for 23 h, and then the glulam specimens were made with the format of 350 mm × 350 mm. The normal section of glulam is shown in Fig.1. The standard specimens were designed and made according to "The wood structure test method standard" (GB/T 50329-2002) and "Plywood" (GB 9846-2004), and tested. The test specimens of static bending strength and elastic modulus test: length * width = 300 mm * 50 mm, loading to failure at the speed of 10 Pa/s. The span is 270 mm, and the test loading mode referenced "man-made board and the veneer panel physico-chemical properties test method" (GB/T1 7657-1999). The static bending strength refers to the pressure intensity that artificial plate can bear in the stress bending to fracture, with the unit of MPa (Nasreen et al., 2015). The test adopted the type of loading in section and plane which can be seen in Fig. 2.

Table 1 Assemble pattern.

Text number	Assemble pattern
1A	Cross assembly of core seven layers wood veneer, parallel assembly of the three layers wood veneers on the two sides
2A	Cross assembly of core seven layers wood veneer, parallel assembly of the three layers wood veneers on the two sides; the half, glass fiber mesh cloth is arranged between the two layers of the wood veneers for reinforce; the other half, aluminum foil is arranged between the two layers of the wood veneers for reinforce
3A	Cross assembly of core seven layers wood veneer, parallel assembly of the three layers wood veneers on the two sides; glass fiber mesh cloth is arranged between the two layers of the wood veneers for reinforce
4A	Cross assembly of core seven layers wood veneer, parallel assembly of the three layers wood veneers on the two sides; aluminum foil is arranged between the two layers of the wood veneers for reinforce
5A	Cross assembly of core seven layers wood veneer, parallel assembly of the three layers wood veneers on the two sides; glass fiber mesh cloth or aluminum foil is arranged between the two layers of the wood veneers for reinforce, wherein the glass fiber grid cloth and aluminum foil distribute at intervals

3. Results and discussion

3.1. Analysis of the effect of EP/wood biocomposites

The average of the 3 parallel specimens of each group was calculated. Test results of 5 specimens are shown in Table 2.

From the data of experimental group 1A, 2A, 3A, and 5A we can know that glass fiber cloth played the role of reinforced EP/wood biocomposites. Under the plane compression, the static bending strength and elastic modulus of laminated timber reinforced with glass fiber cloth increased more than 2 times. Among them, the single glass fiber cloth increased the minimum; under the section compression, the failure load, static elastic modulus and bending strength of EP/wood biocomposites reinforced with glass fiber cloth did not increase significantly. From the data of experimental group 1A, 2A, 4A, and 5A we can know that aluminum foil played the role of reinforced EP/wood biocomposites. Under the plane compression, the static bending strength and elastic modulus of EP/wood biocomposites reinforced with aluminum foil increased more than 2 times. When reinforced with aluminum

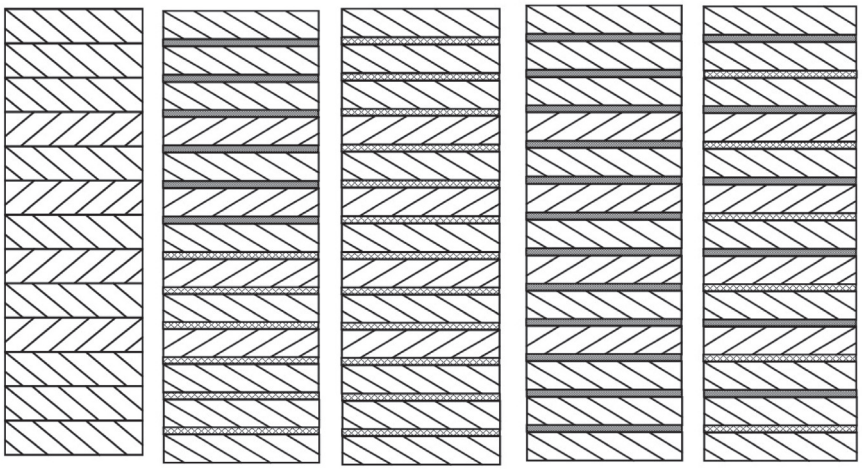

Figure 1 Normal section of the EP/wood biocomposites.

Figure 2 Test load figure of MOR.

Table 2 Test results.

Text number	Plane compression					Section compression				
	Width (mm)	Thickness (mm)	Failing load (N)	MOR (MPa)	Elastic modulus (MPa)	Width (mm)	Thickness (mm)	Failing load (N)	MOR (MPa)	Elastic modulus (MPa)
1A	50.60	27.46	1687	17.91	1770.6	26.68	50.46	7305	43.55	2627.0
2A	51.10	28.84	4555	43.40	3725.4	29.22	50.04	7920	43.84	2607.4
3A	50.72	27.70	4005	41.68	3811.5	28.30	52.90	9620	49.20	2948.2
4A	51.18	25.84	3560	42.19	4708.8	26.08	50.50	8050	49.02	3340.3
5A	51.14	25.16	4525	56.61	5407.1	25.48	50.64	9790	60.68	3658.4

foil alone, the strength of EP/wood biocomposites increased the minimum; under the section compression, the failure load, static elastic modulus and bending strength of EP/wood biocomposites reinforced with aluminum foil did not increase significantly (Liu et al., 2008). We can draw two results from the above analysis: one is that the effect of adding glass fiber cloth, aluminum foil and other reinforcing material is not obvious under the section compression; the other one is that the single enhancement effect of glass fiber cloth and aluminum foil is worse than their composite enhancement effect. At the same time, because the assemble pattern of glass fiber cloth and aluminum foil is different, their enhancement effect is also different (Hashemi et al., 2015). Table 2 shows that the scheme of 5A is the best assemble pattern, namely the composite reinforced way is the cross assembly of core seven layers of wood veneer together with the parallel assembly of the three layers of

wood veneers of the two sides; glass fiber mesh cloth or aluminum foil is arranged between the two layers of the wood veneers for reinforcement, wherein the glass fiber grid cloth and aluminum foil are distributed at intervals (Moody, 1970).

3.2. The base of nonlinear finite element analysis on glulam

Nonlinear finite element analysis is an effective method for predicting the mechanical performance of materials, and the establishment of failure criterion and constitutive equations is the foundation and key for the nonlinear finite element analysis on mechanical condition of materials.

3.3. The failure criterion of glulam

EP/wood biocomposites is the laminated plate formed by overlapping the single plates together in different types. This study used five kinds of experimental components which adopted the cross assembly of core seven layers of wood veneers and were reinforced by aluminum foil, glass fiber grid cloth and the mix of them. Because each of the EP/wood biocomposite layers of fiber alignment is not the same, which may cause the inconsistency of deformation of each layer due to the action of stress, how to decide the final mechanical performance became a very complicated problem. Tsai–Wu tensor criterion is the most comprehensive description of the existing mature standards, and other criteria all can be given by simplifying this criterion according to their own specific loading condition. Tsai–Wu of the original failure criterion boiled down to a higher order tensor polynomial standard, its general form is:

$$F_i\sigma_i + F_{ij}\sigma_i\sigma_j + F_{ijk}\sigma_i\sigma_j\sigma_k + \cdots = 1 \quad i,j,k,\ldots = 1,2,\ldots,6 \tag{1}$$

In this equation, σ_i, σ_i and σ_i are stress vectors; F_i, F_{ij}, F_{ijk} are strength parameters. They are symmetric tensor, and generally can be obtained by experiment. In engineering design, we can usually get the required accuracy by using only the first two of the equation in order to avoid the high experimental expense for determining the tensor coefficients, namely,

$$F_i\sigma_i + F_{ij}\sigma_i\sigma_j = 1 \tag{2}$$

For one-way slab in state of plane stress, it is written in matrix form as:

$$\{F_1 \quad F_2 \quad F_6\}\begin{Bmatrix}\sigma_1\\ \sigma_2\\ \sigma_6\end{Bmatrix} + \{\sigma_1 \quad \sigma_2 \quad \sigma_6\}\begin{bmatrix}F_{11} & F_{12} & F_{16}\\ F_{12} & F_{22} & F_{26}\\ F_{16} & F_{26} & F_{66}\end{bmatrix}\begin{Bmatrix}\sigma_1\\ \sigma_2\\ \sigma_6\end{Bmatrix} = 1 \tag{3}$$

In the principal direction of coordinates of the material, the change of the direction of shear stress will not affect the strength of the material, so the corresponding strength coefficient of the term of the first degree of shear stress in the equation must be zero, namely,

$$F_6 = F_{16} = F_{26} = 0 \tag{4}$$

By substituting it in Eqs. (6)–(12) and expanding it, you can get

$$F_1\sigma_1 + F_2\sigma_2 + F_{11}\sigma_1^2 + F_{22}\sigma_2^2 + F_{66}\sigma_6^2 + 2F_{12}\sigma_1\sigma_2 = 1 \tag{5}$$

In this formula, strength parameters of the first 5 can be obtained through uniaxial tension–compression test and pure shear test along the principal directions of the material, namely

$$\begin{cases} F_1X_t + F_{11}X_t^2 = 1 \quad (\text{only } \sigma_1 > 0, \text{ other stress components are zero})\\ -F_1X_c + F_{11}X_c^2 = 1 \quad (\text{only } \sigma_1 < 0, \text{ other stress components are zero})\\ F_2Y_t + F_{22}Y_t^2 = 1 \quad (\text{only } \sigma_2 > 0, \text{ other stress components are zero})\\ -F_2Y_c + F_{22}Y_c^2 = 1 \quad (\text{only } \sigma_2 < 0, \text{ other stress components are zero})\\ F_{66}S^2 = 1 \quad (\text{only } \sigma_6\ (\tau_{12}) \neq 0, \text{ other stress components are zero}) \end{cases} \tag{6}$$

The strength coefficient F_i and F_{ij} can be solved by the above formula, namely

$$\begin{cases} F_1 = \frac{1}{X_t} - \frac{1}{X_c}, \quad F_{11} = \frac{1}{X_tX_c}\\ F_2 = \frac{1}{Y_t} - \frac{1}{Y_c}, \quad F_{22} = \frac{1}{Y_tY_c}\\ F_{66} = \frac{1}{S^2} \end{cases} \tag{7}$$

By substituting the solution in guidelines Eqs. (1)–(7), you can get

$$\frac{\sigma_1^2}{X_tX_c} + \frac{\sigma_2^2}{Y_tY_c} + \frac{X_c - X_t}{X_tX_c}\sigma_1 + \frac{Y_c - Y_t}{Y_tY_c}\sigma_2 + 2F_{12}\sigma_1\sigma_2 + \frac{\tau_{12}^2}{S^2} = 1 \tag{8}$$

Simplifying the above formula, you can get the Hoffman strength criterion, namely

$$\frac{\sigma_1^2 - \sigma_1\sigma_2}{X_tX_c} + \frac{\sigma_2^2}{Y_tY_c} + \frac{X_c - X_t}{X_tX_c}\sigma_1 + \frac{Y_c - Y_t}{Y_tY_c}\sigma_2 + \frac{\tau_{12}^2}{S^2} = 1 \tag{9}$$

The remaining coefficient F_{12}, which reflected the interaction of the tension–compression strength of the principal direction 1 and 2, can be obtained by biaxial tensile test instead of uniaxial test.

Assuming $\sigma_1 = \sigma_2 = \sigma_0, \sigma_6 = 0$, substituting it in the Eq. (5), there is

$$(F_1 + F_2)\sigma_0 + (F_{11} + F_{22} + 2F_{12})\ \sigma_0^2 = 1 \tag{10}$$

Working out F_{12} to get

$$F_{12} = \frac{1}{2\sigma_0^2}\left[1 - \left(\frac{1}{X_t} - \frac{1}{X_c} + \frac{1}{Y_t} - \frac{1}{Y_c}\right)\sigma_0 - \left(\frac{1}{X_tX_c} + \frac{1}{Y_tY_c}\right)\sigma_0^2\right] \tag{11}$$

Obviously, F_{12} not only depends on basic strength, but is also associated with the biaxial tensile strength. It was noticed that this parameter can be determined by the biaxial tensile test, which is the advantage of Tsai–Wu theory being different from other criteria. But there is also a big problem with that theory, that is, the parameters are very sensitive to the variability of experiment. A minor strength parameter error may lead to a larger variation in parameter value. Therefore, it is necessary to introduce the restrictions on its value (Harvey et al., 1999).

On the other hand, the material will be destroyed when the stress increases to a certain extent. So in stress space, the criterion Eq. (5) should be a closed minimal surface which is called the strength envelope. Its intersection with the plane $\sigma_6 = 0$ is

$$F_1\sigma_1 + F_2\sigma_2 + F_{11}\sigma_1^2 + F_{22}\sigma_2^2 + 2F_{12}\sigma_1\sigma_2 = 1 \tag{12}$$

It should be a closed curve. According to the nature of the quadratic curve, it should be an ellipse instead of a parabola or hyperbola. It should have the following relationship between the coefficients:

$$F_{11}F_{22} - F_{12}^2 > 0 \tag{13}$$

Namely

$$-1 < F_{12}^* = \frac{F_{12}}{\sqrt{F_{11}F_{22}}} < 1 \tag{14}$$

This is the value range of F_{12}^*. For the sake of simplicity, we usually take $F_{12}^* = -0.5$ or 0. The calculated results for most composite materials showed that the difference of the two is less than 10%.

3.4. The constitutive equation

The constitutive relationship of each layer of EP/wood biocomposites can be included in the nonlinear influence of material with the incremental form of Hooke's law, namely

$$\{d\sigma'\}_l = [Q']_l\{d\varepsilon'\} \tag{15}$$

In this formula,

l refers to the l layer of the EP/wood biocomposites;

$\{d\sigma'\}_l = \{d\sigma_x, d\sigma_y, d\tau_{xy}\}$, $\{d\varepsilon'\}_l = \{d\varepsilon_x, d\varepsilon_y, d\gamma_{xy}\}$ is the interlaminar stress increment vector under the assumption that the interlayer of EP/wood biocomposites bonds well;

$\{d\sigma'\}_l = \{d\sigma_x, d\sigma_y, d\tau_{xy}\}$, $\{d\varepsilon'\}_l = \{d\varepsilon_x, d\varepsilon_y, d\gamma_{xy}\}$ is the interlaminar strain increment vector under the assumption that the interlayer of EP/wood biocomposites bonds well;

$[Q']_l$ is the constitutive matrix of the elastic phase, elastic–plastic phase and the subsequent inactive phase for different stress levels. After the superposition of the constitutive equation for each layer, the stress–strain relationship can be formed as following:

$$\{dN\}_l = \sum_{l=1}^{n} [Q']_l t_l \{d\varepsilon'\} \tag{16}$$

Among them, $\{dN\} = \{N_x, N_y, N_{xy}\}$ is the residual force vector operating on the inside of each layer. t_l is the thickness of the plate of the l layer; n is the layers of plates.

3.5. The nonlinear finite element simulation analysis on glulam

Using the specimen size and the loading conditions which are the same with the experiment, through the comparison of the force and displacement for the whole process, simulating and analyzing the factors that have influence on EP/wood biocomposites, and verifying the rationality of finite element simulation analysis at the same time. Anisotropic characteristics of wood and isotropic characteristics of other materials were used in the analysis (Khaskheli et al., 2015). The constitutive model and main parameters of the primary materials were arranged as follows (see Table 3).

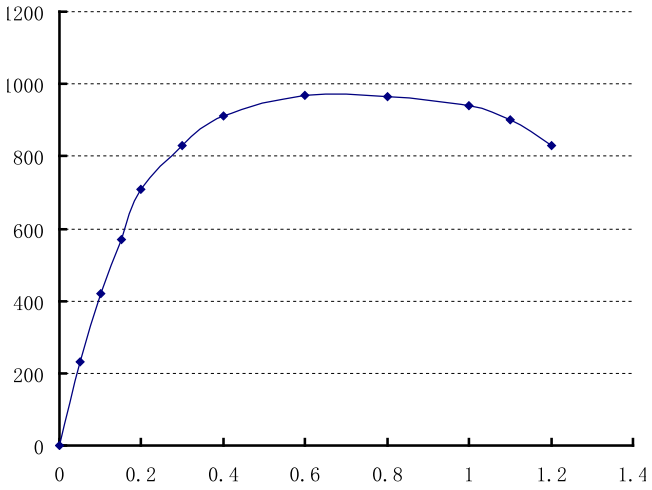

Figure 3 Constitutive relation of GFRP.

(1) The engineering parameters of wood and resin adhesiveAnisotropy of wood: Young's modulus $E_1 = E_2 = E_3 = 1000$ MPa, Poisson's ratio $NU_{12} = NU_{13} = 0.4$, $NU_{23} = 0.04$, shear modulus $G_{12} = G_{13} = 100$, $G_{23} = 50$ (see Fig. 3).The isotropic epoxy resin adhesive: Young's modulus $E = 1{,}000{,}000$, shear modulus $G_1 = G_2 = 1{,}000{,}000$, the viscous coefficient for 1.0e–5.
(2) The constitutive relations of materials reinforced with glass fiberIsotropy, Young's modulus 7000 MPa, Poisson's ratio of 0.22.
(3) The constitutive relations of materials reinforced with aluminum foilIsotropy, Young's modulus 72,000 MPa, Poisson's ratio of 0.33 (see Fig. 4).

3.6. The division of units and the specimen failure conditions

The failure occurred mainly in midspan and at the end of supports where the stress is concentrative. In order to improve the speed and precision of the numerical analysis, the test specimens were divided into 5 sections. Wherein both ends and the midspan each accounted for 1/10 of the specimen, using smaller units, while the other parts used relatively large units. From the results of numerical analysis, it is very difficult to simulate the fracture failure situation of the specimens which mainly is the glue failure (see Fig. 5).

Table 3 Setting value of component thickness and span.

Assemble pattern	$l(h = 54)$					$l(h = 27)$				
Non-reinforced materials	270	320	370	420	470	270	320	370	420	470
Reinforced with glass fiber and aluminum foil each half	270	320	370	420	470	270	320	370	420	470
Reinforced with glass fiber	270	320	370	420	470	270	320	370	420	470
Reinforced with aluminum foil	270	320	370	420	470	270	320	370	420	470
Reinforced with the interleaving of glass fiber and aluminum foil	270	320	370	420	470	270	320	370	420	470

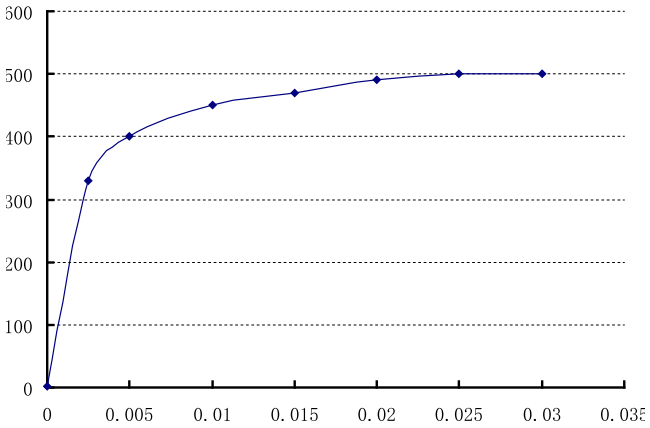

Figure 4 Constitutive relation of aluminum foil reinforcement.

3.7. The experiment and the comparison of simulation results

The results of the test and analysis of a section compression and a plane compression in the whole process were compared, as shown in Figs. 6 and 7. The test results showed that from loading to yield, and to the specimen failure, there is some fluctuation in the load-midspan deformation curve (Batool et al., 2015). The failure of the primary timber and reinforced materials has a progressive process and a process of redistribution and transmission of the internal force. The results of finite element numerical analysis are relatively ideal, the load-midspan deformation curve was a straight line from loading to yield. After the yield, the curve showed a horizontal linear development, with almost no decline. From the comparison of the load-midspan deformation curve of the two, the numerical analysis results agreed well with experimental results, especially the relative error in ultimate bearing capacity and ultimate deformation is small, which proved it's feasible and effective to analyze parameters through numerical simulation analysis (Peng et al., 2013a,b,c).

By using the displacement loading, and controlling the ultimate displacement of the midspan and the experimental test to make they are the same, analyzing the test data of the 10 groups with the numerical simulation method. The comparison of results of the ultimate bearing capacity of numerical analysis and experimental test is shown in Table 4. The results of numerical analysis grew large overall, and the possible reasons are: the constraint condition of supports in numerical simulation is difficult to remain the same as the situation of supports in the experimental test; the constitutive relation of material does not match the actual situation; the contact simulation of colloidal material, reinforced materials and wood veneer has disparity with the actual situation (Spence, 2002).

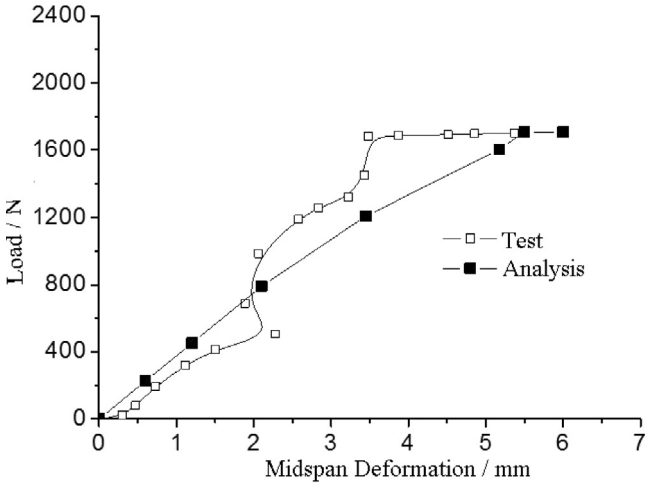

Figure 6 Load and deformation of sample, 2A under flat pressure.

3.8. Nonlinear finite element analysis on numerical parameters of glulam

Through the nonlinear finite element analysis on numerical parameters for the assemble thickness of variation tests and the length of specimens, the general variation law was obtained and the displacement loading was used to analyze the ultimate bearing capacity, as shown in Table 5.

According to the assemble pattern of the test 1A, the relationships between the length and thickness of glued timber members with the whole wood veneer are shown in Fig. 8. Fig. 8 shows that while the thickness remains the same, the bearing capacity decreased gradually with the increase of the member length; while the length remains the same, the bearing capacity increased with the increase in the thickness of the member, and the thicker, the greater the gap between flat pressure and side pressure, which is consistent with the stress nephogram. Simulation results show that in EP/wood biocomposites for bridges, the plane compression mode should be chosen, which is consistent with the experimental results (Peng et al., 2014a,b) (see Fig. 9).

In terms of the assemble pattern of 2A, the relationship between the length and thickness of glass fiber cloth reinforced glulam member and the stress is shown in Fig. 10. Fig. 10 shows that while the thickness is the same, the bearing capacity decreased gradually with the increase in member length; while the length is the same, the bearing capacity increased with the increase in the thickness of the member, and for the thickness of 27 mm, the bearing capacity under side pressure is larger than that under flat pressure, while the bearing capacity under

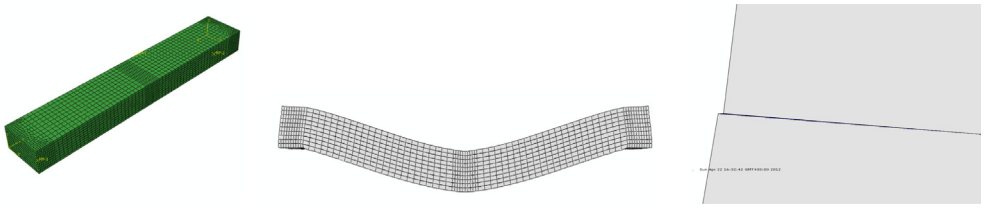

Figure 5 Component stress unit.

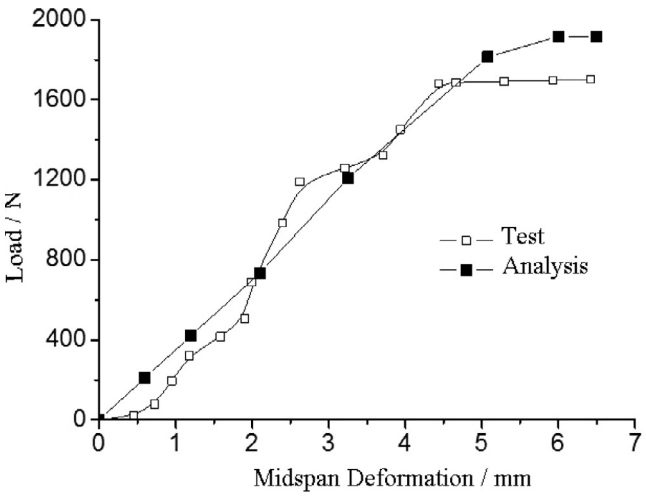

Figure 7 Load and deformation of sample, 2A under side pressure.

flat pressure is two times that under side pressure for the thickness of 54 mm. The simulation results showed that the flat pressure mode should be chosen for the EP/wood biocomposites used in long-span bridges, which is consistent with the experimental results; and the side pressure mode should be chosen for the EP/wood biocomposites used in short-span bridges. Compared with the Fig. 8, glass fiber cloth possesses the enhancement effect, which is in agreement with the result of the experiment.

In terms of the assemble pattern of 3A, the relationship between the length and thickness of aluminum foil reinforced glulam member and the stress was shown in Fig. 11. Fig. 11 shows that while the thickness is the same, the bearing capacity decreased gradually with the increase of member length; while the length is the same, the bearing capacity increased with the increase of the thickness of the member, and for the thickness of 27 mm, the bearing capacity under side pressure is nearly equal to that under flat pressure, while the bearing capacity under flat pressure is more than two times that under side pressure for the thickness of 54 mm. The simulation results showed that the flat pressure mode should be chosen for the EP/wood biocomposites used in bridges, which is consistent with the experimental results. Compared with the Fig. 8, aluminum foil possesses the enhancement effect, which is in agreement with the result of the experiment. Compared with the Fig. 10, the enhancement effect of aluminum foil is better than that of glass fiber cloth, which differs from the experimental results. It is because the simulation results are based on the amalgamation of the bonding interface of aluminum foil and epoxy resin. Meanwhile, it also showed that the bearing capacity of EP/wood biocomposites will get a promotion by improving the fusion of the bonding interface of aluminum foil and epoxy resin (Wang et al., 2003).

In terms of the assemble pattern of 4A, the relationship between the length and thickness of glass fiber cloth and aluminum foil composite glulam member and the stress was shown in Fig. 12. Fig. 12 shows that while the thickness is the same, the bearing capacity decreased gradually with the increase in member length; while the length is the same, the bearing capacity increased with the increase in the thickness of the member, and for the thickness of 27 mm, the bearing capacity under side pressure is nearly equal to that under flat pressure, while the bearing capacity under flat pressure is nearly two times that under side pressure for the thickness of 54 mm. The simulation results showed that the flat pressure mode should be chosen for the EP/wood biocomposites used in long-span bridges, which is consistent with the experimental results; and the side pressure mode should be chosen for the EP/wood biocomposites used in short-span bridges. Compared with the Fig. 10 and the Fig. 11, when the thickness is 27 mm, the bearing capacity of the two is almost the same under flat pressure; when the thickness is 54 mm, aluminum foil reinforced effect > aluminum foil and glass fiber composite reinforced effect > glass cloth reinforced effect. Under the side pressure, glass cloth reinforced effect > aluminum foil and glass fiber composite reinforced effect > aluminum foil reinforced effect.

In terms of the assemble pattern of 5A, the relationship between the length and thickness of glass fiber cloth and aluminum foil composite glulam member and the stress is shown in Fig. 13. Fig. 13 shows that while the thickness is the same, the bearing capacity decreased gradually with the increase of member length; while the length is the same, the bearing capacity increased with the increase in the thickness of the member, and for the thickness of 27 mm, the bearing capacity under side pressure is nearly equal to that under flat pressure, while the bearing capacity under flat pressure is nearly two times that under side pressure for the thickness of 54 mm. The simulation results showed that the flat pressure mode should be chosen for the EP/wood biocomposites used in long-span bridges, which is consistent with the experimental results; and the side pressure mode should be chosen for the EP/wood biocomposites used in short-span bridges. Compared with the Fig. 10 and the Fig. 11, when the thickness is 27 mm, the bearing capacity of the two is almost the same under flat pressure; when the thickness is 54 mm, aluminum foil reinforced effect > aluminum foil and glass fiber composite reinforced effect > glass

Table 4 Analysis of simulation values compared with test results.

Flat pressure				Side pressure			
Test number	Experimental value	The simulation value	Relative error	Test number	Experimental value	The simulation value	Relative error
1A	1710	1708	0.12%	1A	1421	1625	−14.36%
2A	1702	1917	−12.63%	2A	1679	1893	−12.75%
3A	1687	2193	−29.99%	3A	1685	1790	−6.23%
4A	1258	1545	−22.81%	4A	1687	1657	1.78%
5A	1687	1932	−14.52%	5A	1867	1961	−5.03%

Table 5 Finite element simulation results.

Thickness (mm)	Span (mm)	Compression mode	Bearing capacity (N)				
			1A	2A	3A	4A	5A
27	270	Flat pressure	1421	1679	1685	1687	1867
	270		1625	1893	1790	1657	1961
	320		1262	1435	1197	1546	1332
	370		890	1019	835	1109	941
	420		652	746	603	829	687
	470		488	561	449	628	515
54	270		6236	7058	6585	7357	6881
	320		3906	5386	4846	5673	5220
	370		2395	4192	3694	4459	4040
	420		1543	3316	2870	3559	3181
	470		1053	2661	2266	2880	2543
27	270	Side pressure	1710	1702	1687	1258	1687
	270		1708	1917	2193	1545	1932
	320		1192	1289	1483	1020	903
	370		840	899	1044	703	901
	420		388	648	759	504	649
	470		311	481	568	372	482
54	270		3418	4018	4433	3191	4033
	320		1840	2769	2997	2105	2704
	370		875	1930	2108	1452	1878
	420		472	1391	1532	1039	1351
	470		315	1032	1145	768	1001

Note: Assemble pattern of 1A: full-wooden; assemble pattern of 2A: AL-G; assemble pattern of 3A: G-G; assemble pattern of 4A: AL-AL; assemble pattern of 5A: AL-G-AL-G.

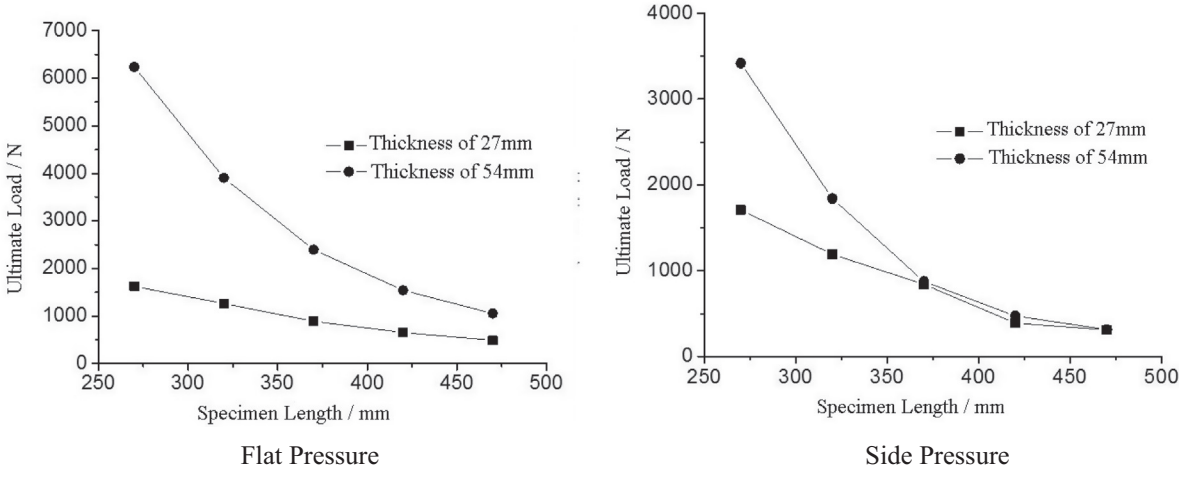

Figure 8 Relations between length, thickness and load of wooden glulam.

cloth reinforced effect. Under the side pressure, glass cloth reinforced effect > aluminum foil and glass fiber composite reinforced effect > aluminum foil reinforced effect. Compared with the Fig. 12, when the thickness is 27 mm, the bearing capacity of the two is almost the same under flat pressure; when the thickness is 54 mm, reinforced effect of the semi-assembling of glass fiber and aluminum foil is superior to reinforced effect of the cross-assembling of glass fiber and aluminum foil. Under the side pressure, reinforced effect of the semi-assembling of glass fiber and aluminum foil is almost equal to the reinforced effect of the cross-assembling of glass fiber and aluminum foil, which is different from the experimental results. The specific reasons need to be further studied (Wang et al., 2013).

In summary, aluminum foil and glass fiber cloth both possess the enhancement effect; the span of specimen increased, then the ultimate bearing capacity decreased; the thickness of assemble specimen is large, the ultimate bearing capacity is large too; while the thickness of specimens is different from each other, the length increased, then the gap of the ultimate bearing capacity of specimens reduced gradually, which indicates that the thickness and length have interactive effects on the ultimate load capacity. This is consistent with the experimental results (Sultana et al., 2015).

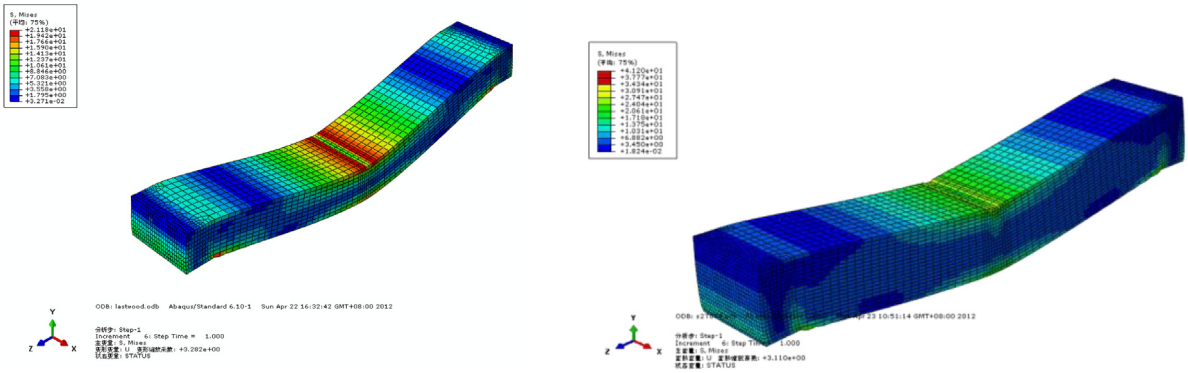

The thickness of 27mm The thickness of 54mm

Figure 9 Mise stress diagram of wooden glulam with span 270 mm.

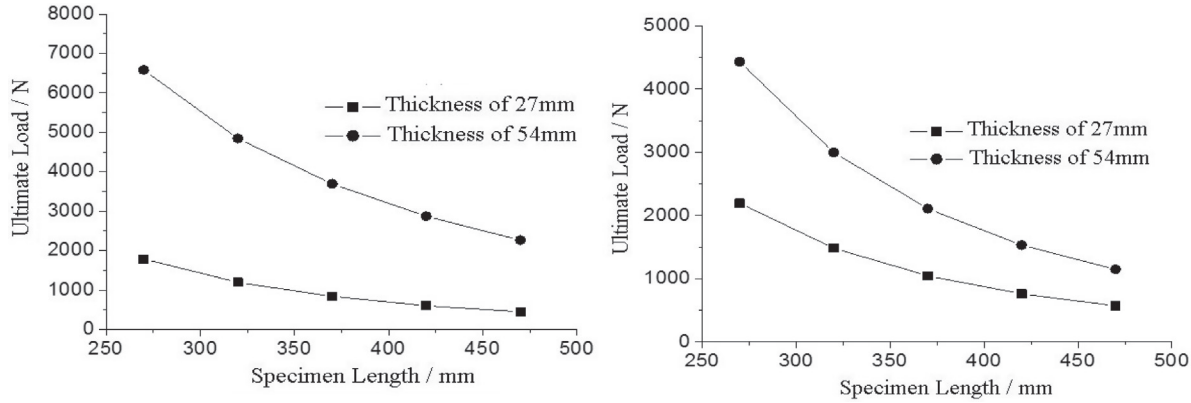

Figure 10 Relations between length, thickness and load of wood–GFRP glulam.

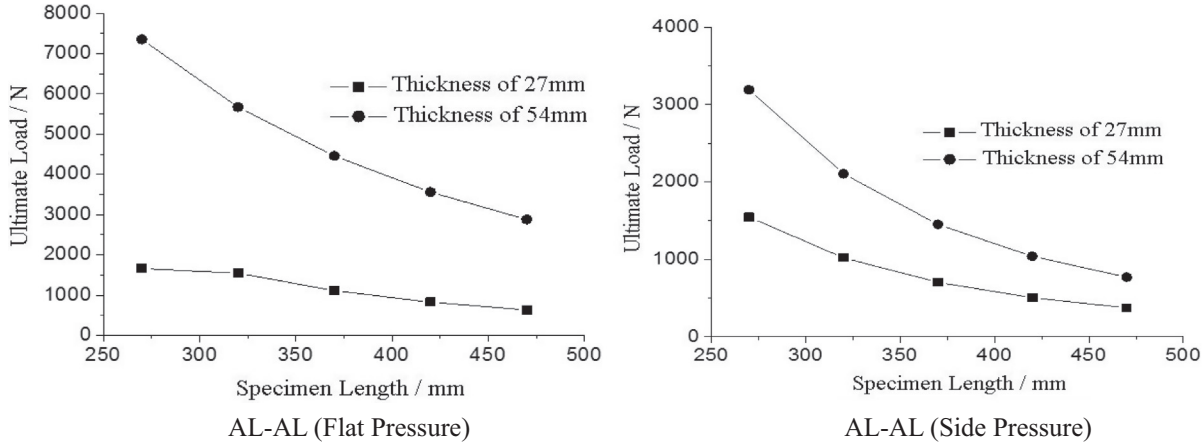

Figure 11 Relations between length, thickness and load of wood–aluminum glulam.

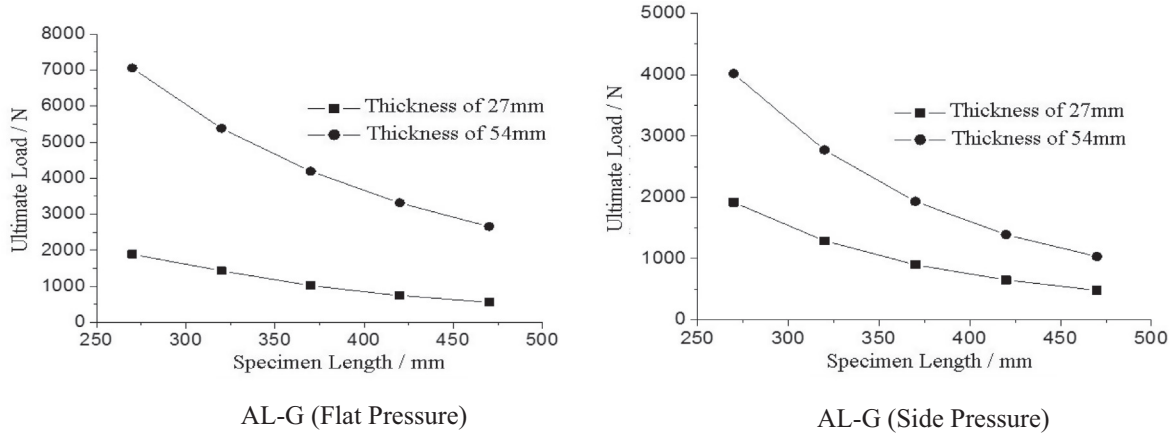

Figure 12 Relations between length, thickness and load of wood–GFRP–aluminum glulam.

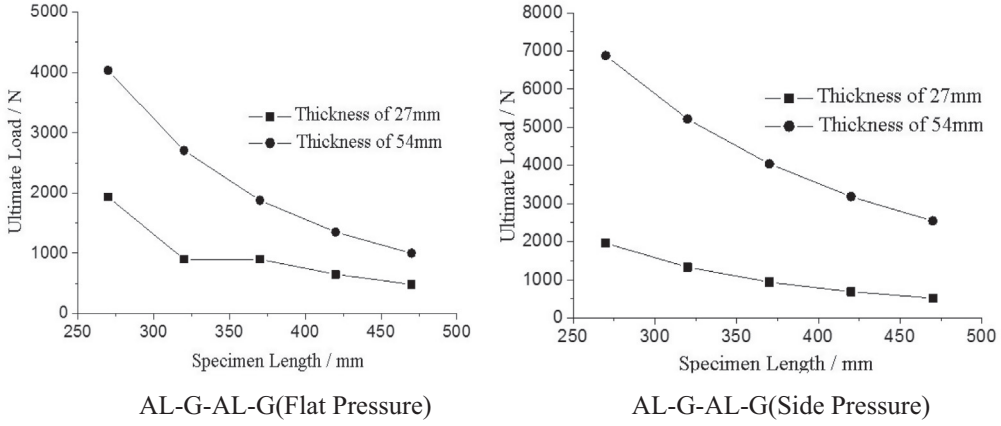

Figure 13 Relations between length, thickness and load of wood–GFRP–aluminum glulam.

4. Conclusion

(1) Under the flat pressure, reinforced effect of glass fiber, aluminum foil is not obvious; Under the side pressure, glass fiber cloth or aluminum foil single reinforced effect is worse than aluminum foil and glass fiber composite reinforced effect; at the same time, the enhancement effect of glass fiber cloth, aluminum foil is also different while the assemble pattern is different, wherein the scheme of 5A is the best assemble pattern, namely the composite reinforced way is the cross assembly of core seven layers of wood veneer together with the parallel assembly of the three layers of wood veneers of the two sides; glass fiber mesh cloth or aluminum foil is arranged between the two layers of the wood veneers for reinforcement, wherein the glass fiber grid cloth and aluminum foil are distributed at intervals (Javed et al., 2015).

(2) Through the nonlinear finite element analysis, we got the failure criterion equation of glulam: $F_{12} = \frac{1}{2\sigma_0^2}\left[1 - \left(\frac{1}{X_t} - \frac{1}{X_c} + \frac{1}{Y_t} - \frac{1}{Y_c}\right)\sigma_0 - \left(\frac{1}{X_t X_c} + \frac{1}{Y_t Y_c}\right)\sigma_0^2\right]$, the relationship between the coefficients is: $-1 < F_{12}^* = \frac{F_{12}}{\sqrt{F_{11}F_{22}}} < 1$, and the constitutive relation equation of glulam layers is: $\{dN\}_l = \sum_{l=1}^{n}[Q']_l t_l \{d\varepsilon'\}$.

(3) The finite element simulation results of nonlinear showed that aluminum foil and glass fiber cloth both possess the enhancement effect; the span of specimen increased, then the ultimate bearing capacity decreased; the thickness and length of assemble specimen is large, the ultimate bearing capacity is large too, and the thickness and length have interactive effect on the ultimate load capacity. This is consistent with the experimental results (Khan et al., 2015).

Acknowledgment

Foundation Item: National Introduction of International Advanced Forestry Science and Technology Projects (2012-4-27); Program for New Century Excellent Talents (NCET-12-0725).

References

Barreto, A.M.J.P., Campilho, R.D.S.G., DeMoura, M.F.S.F., 2010. Repair of wood trusses loaded in tension with adhesively bonded carbon-epoxy patches. J. Adhes. 86 (5–6), 630–648.

Batool, S., Khalid, A., Chowdury, A.J.K., Sarfraz, M., Balkhair, K.S., Ashraf, M.A., 2015. Impacts of azo dye on ammonium oxidation

process and ammonia oxidizing soil bacteria. RSC Adv. 5, 34812–34820. http://dx.doi.org/10.1039/C5RA03768A.

Hashemi, S.S.G., Mahmud, H.B., Ashraf, M.A., 2015. Performance of green roofs with respect to water quality and reduction of energy consumption in tropics: a review. Renewable Sustainable Energy Rev. 52 (2015), 669–679.

Hernandez, R., Davalos, J.F., Sonti, S.S., 1997. Strength and stiffness of reinforced yellow-poplar glued-laminated beams. FSRP-FPL-554, p. 38.

Harvey, B., Blankenhorn, P.R., Janowiak, J.J., 1999. Northern red oak glued-laminated timber bridge. J. Bridge Eng. 4 (4), 269–278.

Javed, I., Mateen, F., Rafique, U., Tabassum, N., Balkhair, K.S., Ashraf, M.A., 2015. Synthesis of zeolite from marble powder waste: a greener approach and its application for the removal of inorganic metals from wastewater. Desalin. Water Treat. 2015, 1–10. http://dx.doi.org/10.1080/19443994.2015.1033763.

Khan, A.M., Ahmad, C.S., Farooq, U., Mahmood, K., Sarfraz, M., Balkhair, K.S., Ashraf, M.A., 2015. Removal of metallic elements from industrial waste water through biomass and clay. Front. Life Sci., 1–8, http://wwwtandfonline.com/doi/full/10.1080/21553769.2015.1041187.

Khaskheli, A.A., Talpur, F.N., Ashraf, M.A., Cebeci, A., Jawaid, S., Afridi, H.I., 2015. Monitoring the *Rhizopus oryzae* lipase catalyzed hydrolysis of castor oil by ATR-FTIR spectroscopy. J. Mol. Catal. B: Enzym. 113, 56–61. http://dx.doi.org/10.1016/j.molcatb.2015.01.002.

Liu, Q.M., Luo, Y.S., Yin, S.P., Chen, S.M., Zhang, D.Q., Peng, W.X., 2008. Liquid rheology study on refined rapeseed oil. J. Central South Univ. Technol. 15, 525–528.

Mateen, F., Javed, I., Rafique, U., Tabassum, N., Sarfraz, M., Safi, S.Z., Yusoff, I., Ashraf, M.A., 2015. New method for the adsorption of organic pollutants using natural Zeolite Incinerator Ash (ZIA) and its application as an environmentally friendly and cost-effective adsorbent. Desalin. Water Treat. 2015, 1–9. http://dx.doi.org/10.1080/19443994.2015.100514.

Moody, R.C., 1970. Glued-EP/wood biocomposites research at the forest products laboratory. For. Prod. J. 20 (9), 81–86.

Nasreen, S., Rafique, U., Ehrman, S., Ashraf, M.A., 2015. Hybrid mesoporous silicates: a distinct aspect to synthesis and application for decontamination of phenols. Saudi J. Biol. Sci. http://dx.doi.org/10.1016/j.sjbs.2015.08.014.

Peng, W.X., Wang, L.S., Wu, F.J., Xu, Q., 2011. 3-(4-Bromophenyl)-4-(4-hydroxyanilino)furan-2(5H)-one. Acta Crystallogr., Sect. E: Struct. Rep. Online 67, O2329-U206.

Peng, W.X., Wang, L.S., Xu, Q., Wu, Q.D., Xiang, S.L., 2012a. TD-GC–MS Analysis on thermal release behavior of poplar composite biomaterial under high temperature. J. Comput. Theor. Nanosci. 9 (9), 1431–1433.

Peng, W.X., Wu, F.J., Wang, L.S., Xu, Q., 2012b. Crystal structure of 3-(4-bromophenyl)-4-(4-chlorophenylamino)furan-2(5H)-one $C_{16}H_{11}BrClNO_2$. Z. Kristallogr. New Cryst. Struct. 227 (1), 61–62.

Peng, W.X., Le, C., 2012. Crystal structure of 3-(3-bromophenyl)-4-(3 5-dichloro-phenylamino)furan-2(5H)-one $C_{16}H_{10}BrCl_2NO_2$. Z. Kristallogr. New Cryst. Struct. 227 (2), 267–268.

Peng, W.X., Wang, L.S., Lin, Z., Minglong, Zhang, M.L., 2013a. Identification and chemical bond characterization of wood extractives in three species of eucalyptus biomass. J. Pure Appl. Microbiol. 7, 67–73.

Peng, W.X., Wang, L.S., Zhang, M.L., Lin, Z., 2013b. Molecule characteristics of *Eucalyptus* hemicelluloses for medical microbiology. J. Pure Appl. Microbiol. 7 (2), 1345–1349.

Peng, W.X., Lin, Z., Chang, J.B., Gu, F.L., Zhu, X.W., 2013c. Biomedical molecular characteristics of YBSJ extractives from *Illicium verum* fruit. Biotechnol. Biotechnol. Equip. 27 (6), 4311–4316.

Peng, W.X., Wang, L.S., Zhang, M.L., Lin, Z., 2014a. Separation characteristics of lignin from *Eucalyptus Camaldulensis* lignincelluloses for biomedical cellulose. Pak. J. Pharm. Sci. 27, 723–728.

Peng, W.X., Ge, S.B., Li, D.L., Mo, B., Daochun, Q., Ohkoshi, M., 2014b. Molecular basis of antibacterial activities in extracts of *Eucommia Ulmoides* wood. Pak. J. Pharm. Sci. 27 (6), 2133–2138.

Qureshi, T., Memon, N., Memon, S.Q., Ashraf, M.A., 2015. Decontamination of ofloxacin: optimization of removal process onto sawdust using response surface methodology. Desalin. Water Treat. 2015, 1–9. http://dx.doi.org/10.1080/19443994.2015.1006825.

Rasheed, A., Farooq, F., Rafique, U., Nasreen, S., Ashraf, M.A., 2015. Analysis of sorption efficiency of activated carbon for removal of anthracene and pyrene for wastewater treatment. Desalin. Water Treat. 2015, 1–6. http://dx.doi.org/10.1080/19443994.2015.1015304.

Spence, M., 2002. Bridging the credibility gap. Developing the use of treated softwoods for timber bridge structures. J. Inst. Wood Sci. 16 (1), 4–26.

Sultana, N., Akib, S., Ashraf, M.A., Abidin, M.R.Z., 2015. Quality assessment of harvested rainwater from green roofs under tropical climate. Desalin. Water Treat. 2015, 1–8. http://dx.doi.org/10.1080/19443994.2015.1015307.

Wang, L.S., Peng, W.X., Zhang, M.L., Lin, Z., 2013. Separation characteristics of lignin from eucalyptus lignincellulose for medicinal biocellulose preparation. J. Pure Appl. Microbiol. 7, 59–66.

Wang, X., Jiang, Z., Fei, B., 2003. Discussion on several problems of eucalyptus plantation in machining process. World For. Res. 16 (13), 62–64.

Xiao, Z.P., Peng, Z.Y., Dong, J.J., Deng, R.C., Wang, X.D., Ouyang, H., Yang, P., He, J., Wang, Y.F., Zhu, M., Peng, X.C., Peng, W.X., Zhu, H.L., 2013. Synthesis molecular docking and kinetic properties of beta-hydroxy-beta-phenylpropionyl-hydroxamic acids as helicobacter pylori urease inhibitors. Eur. J. Med. Chem. 68, 212–221.

Yin, Y., Jiang, X., Lv, X., 2001. The status of resources and wood utilization of eucalyptus plantation in China. Tim. Ind. 15 (5), 3–5.

Youngquist, J.A., Gromala, D.S., Jokerst, R.W. 1979. Design, fabrication, testing and installation of a press-lam bridge. FSRP-FPL-332, p. 24.